Biointerface Research in Applied Chemistry
Open-Access Journal (ISSN: 2069-5837)

Article
Volume 14, Issue 2, 2024, 35
https://doi.org/10.33263/BRIAC142.035

Stable Hydrophobicity of ZnO Nanorods for Self-Cleaning Materials Using SILAR-CBD Method

Ari Sulistyo Rini [1,*], Herna Herna [1], Yolanda Rati [2], Yan Soerbakti [1]

[1] Department of Physics, Universitas Riau, Simpang Baru 28293, Pekanbaru, Indonesia
[2] Department of Physics, Institut Teknologi Bandung, Ganesa 10, 40132 , Bandung, Indonesia
* Correspondence: ari.sulistyo@lecturer.unri.ac.id (A.S.R.);

Scopus Author ID 36059915000
Received: 12.02.2023; Accepted: 24.06.2023; Published: 4.02.2024

Abstract: The necessity for self-cleaning materials has increased with the demand for hygiene, self-disinfecting, and contamination-free surfaces. In this work, self-cleaning films based on zinc oxide (ZnO) nanorods were prepared by the successive ionic layer adsorption reaction (SILAR) and chemical bath deposition (CBD) techniques with growth times of 0, 3, 6, and 9 hours. UV-Vis Spectroscopy, FESEM, and XRD were used to characterize the optical, morphology, and structural properties. The ZnO peak absorption exists at 245 – 285 nm with the highest transmittance up to 91%. The thickness of the film increases with the duration of the growing process. FESEM images show a nanorod with a hexagonal cross-section and, at the growth time of 6 hours, has the most regular and homogeneous structure with a size of 169.57 ± 25.78 nm. The wurtzite hexagonal structure confirms the ZnO nanorod with a crystallite size of 39.98 nm. ZnO nanorod was applied as self-cleaning material by the sessile drop technique. The hydrophobic surface was obtained at the growth time of 6 hours with a water contact angle of 95.7º, which acts as a self-cleaning material. Therefore, this material has significant industrial application potential as a self-cleaning material.

Keywords: hexagonal; hydrophobic; nanorod; self-cleaning; zinc oxide.

1. Introduction

A self-cleaning technology is one of the innovations currently being developed. Self-cleaning is inspired by biological phenomena such as lotus leaves, taro leaves, gecko feet, and cricket wings with natural self-cleaning mechanisms [1]. It can serve the surface of an object free from dirt or dust contamination [2]. Hydrophobic surfaces' self-cleaning properties are important in medical, textile, engineering, rubber, plastics, and glass [3–5]. Many companies have commercialized several multi-purpose self-cleaning products, one of them is window glass [6]. Construction materials such as tiles, concrete, glass, and paint have used self-cleaning technology [7, 8].

Self-cleaning technology has been developed using several materials, including TiO_2, SiO_2, CuO, and ZnO. Some of these materials have weaknesses, such as TiO_2 being easy to remove from the substrate surface [9], SiO2 having a low thermal conductivity [10], and CuO being only used on inorganic substrates [11]. Therefore, ZnO was chosen for self-cleaning applications because it has stable hydrophobicity, high chemical stabilization, and can control the particle size in the nanometer range [12–14]. ZnO thin film can decompose bacteria and hazardous organic compounds that commonly pollute the environment [15].

Zinc oxide (ZnO) is an inorganic compound from group IIB-VIA metal oxide semiconductor materials [16]. ZnO is in great demand because it has unique properties such as wide bandgap energy (3.37 eV), high melting point (2.248 K) [17], strong ultraviolet emission at room temperature [18], high electron binding energy (60 meV), high thermal conductivity, stable and non-toxic [19]. It can be produced at low or high temperatures at inexpensive [20]. Therefore, ZnO has many applications in catalysts, optoelectronics, and solar cells [21–23]. ZnO nanostructure has various forms, such as nanotubes, nanosheets, and nanowires [24, 25].

The physical properties and surface modification of a material in the form of a thin film can be controlled by the synthesis process and conditions [26]. Several methods are used for the preparation of thin films, including magnetron sputtering [27], atomic layer deposition [28], and chemical vapor deposition [29]. These methods require very high vacuum, expensive equipment, and costs, are carried out at high temperatures, and use toxic gas compounds [30, 31]. The chemical bath deposition (CBD) method, which is conducted by immersing the substrate in the precursor, is often found in the preparation of thin films [32]. Some of its advantages are being able to control the growth factor of nanomaterials (such as pH, temperature, immersion time, and concentration), does not require high-voltage equipment, and can be carried out at low temperatures (< 100°C) [33].

However, the growth of nanomaterials by this method can be disturbed by the homogeneous reaction in the solution during the surface deposition of thin films. This problem can be overcome through pre-treatment by forming a seed layer using the successive ionic layer adsorption reaction (SILAR) method [34]. The SILAR method is based on the adsorption and reaction of ions from the solution and rinsing between each immersion with water to avoid homogeneous settling in the solution. It has the advantages of being cost-effective, can be used on various types of substrates, does not require a vacuum chamber, and can control the thickness of the film [35].

In this work, ZnO was synthesized using two combined methods, SILAR and CBD, on a glass substrate. ZnO samples are prepared with different growth times to control the film's morphology and thickness, which can affect the physical properties. The effect of sample growth time was analyzed on the physical properties of ZnO, namely light absorption, morphology, crystal structure, and hydrophobic properties. Furthermore, it was applied as a self-cleaning material to know the hydrophobic properties of ZnO by measuring the water contact angle using the sessile drop method. The sessile drop was chosen because it is easy to do by utilizing digital image technology on smartphone cameras.

2. Materials and Methods

2.1. Materials.

The materials used in this research were zinc sulfate heptahydrate ($Zn(SO_4)\cdot 7H_2O$) as a seed solution purchased from Supelco, Ammonia hydroxide (NH_4OH,25%) purchased from Emsure as a cationic precursor, zinc nitrate hexahydrate ($Zn(NO_3)_2.6H_2O$) as growth solution purchased from Smart Lab, hexamethylenetetramine ($(CH_2)_6N_4$) as surfactant purchased from Sigma-Aldrich, aquades, acetone (C_3H_6O), and ethanol (C_2H_5OH) as chemical solvents.

2.2. Synthesis of ZnO nanorods.

First, the glass substrate was cleaned in aquades, acetone, and ethanol immersed for 15 minutes using an ultrasonic cleaner. Then, it was immersed in 50 ml $Zn(SO_4).7H_2O$ (10 mM) and NH_4OH for 40 s and in water for 20 s. Furthermore, it was sonicated for 60 s, immersed in water at 80°C for 20 s, and heated at 100°C for 3 minutes. To obtain a homogeneous ZnO seed, this process was repeated in 20 cycles. The seeding mechanism was carried out as in previous research [36]. ZnO seed was annealed using a furnace at a temperature of 250°C for 1 h and grown in 50 mM of $Zn(NO_3)_2 \cdot 6H_2O$ and $(CH_2)_6N_4$ (equimolar) using a water bath at 80°C. The growth time was varied for 0, 3, 6, and 9 hours.

2.3. Characterization.

Specord 200 Plus UV-Vis spectrophotometer was used to characterize the absorbance spectrum of ZnO. The structural properties were analyzed using an Xpert Pro PANalytical type diffractometer. Surface morphology is known from FESEM, type FEI Quanta FEG 650.

2.4. Self-cleaning examination.

About 5 µl of water was dripped onto the ZnO surface. Then, the contact angle of the water is measured by taking pictures using the Angulus application on a smartphone. The sample that has the ability to self-clean is hydrophobic with a water contact angle exceeding 90°.

3. Results and Discussion

3.1. Optical properties.

The UV-Vis absorption curve of the ZnO sample is shown in Figure 1 (a). The maximum absorption intensity is found at 200 – 300 nm in the UV spectrum. Meanwhile, the minimum absorption intensity is at 300 – 600 nm in the visible light spectrum. The length of time for growth causes a shift in the ZnO absorption peak towards a longer wavelength (redshift), namely 245 nm, 250 nm, 285 nm, and 300 nm for each sample Z-0, Z-3, Z-6, and Z-9. It is due to an increase in the size of the thin film as the growth time increases [19].

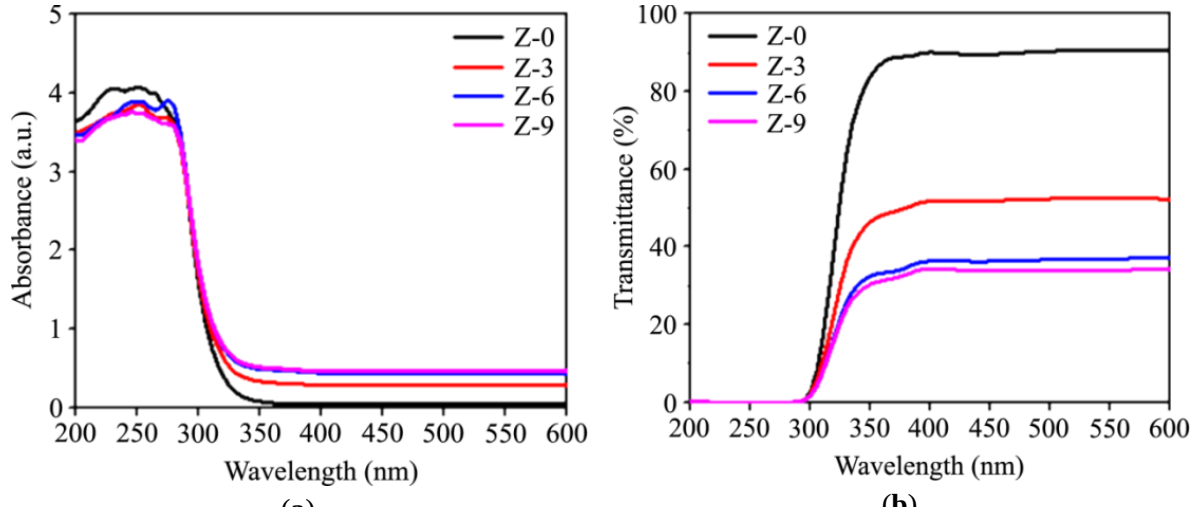

Figure 1. (**a**) Absorbance; (**b**) Transmittance spectra of ZnO with different growth times.

The transmittance spectrum of the ZnO sample is shown in Figure 1 (b). The highest transmittance of Z-0, Z-3, Z-6, and Z-9 samples were 90.61%, 52.83%, 36.99%, and 34.94%, respectively. The low transmittance at 200 – 300 nm is due to the denser constituent atoms resulting in the more frequent collisions of light particles with the atoms making up the layer so that light is difficult to pass through the layer [37]. Transmittance at a wavelength of 300 – 600 nm is constant because electrons cannot absorb the energy of the photons emitted at that wavelength, so the energy given is only transmitted [38].

Besides that, the bandgap energy of the ZnO samples was also studied. The value of band gap energy is known from the extrapolation of the $(\alpha h\upsilon)^2$ vs. hυ curve using the Tauc Plot method in Figure 2.

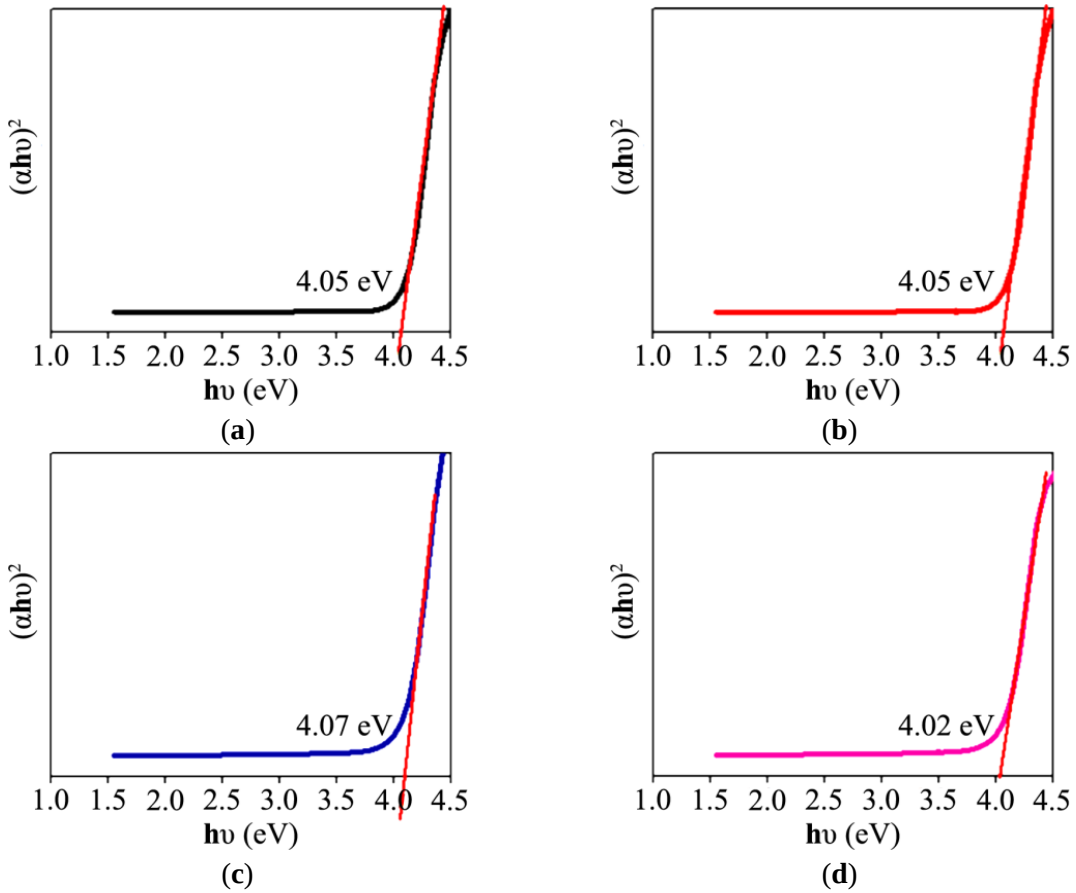

Figure 2. Curve $(\alpha h\upsilon)^2$ vs hυ of ZnO for (**a**) Z-0, (**b**) Z-3, (**c**) Z-6, and (**d**) Z-9.

The band gap energy of the ZnO samples obtained ranges from 4.02 – 4.07 eV. These results show that variations in growth time do not significantly affect photon absorption, especially in the UV spectrum. Sample Z-6 has the highest bandgap energy of 4.07 eV. The band gap energy is relatively large because the sample size is on the nanometer scale [16].

3.2. Surface morphology.

The surface morphology of the ZnO sample with a magnification of 10,000 times is presented in Figure 3. The geometry of the samples Z-3, Z-6, and Z-9 grown on a glass substrate is nanorod hexagonal. Overall, the shape of the nanorod is not uniform, which is thought to be due to distortion of the shift in the diffraction peaks [39].

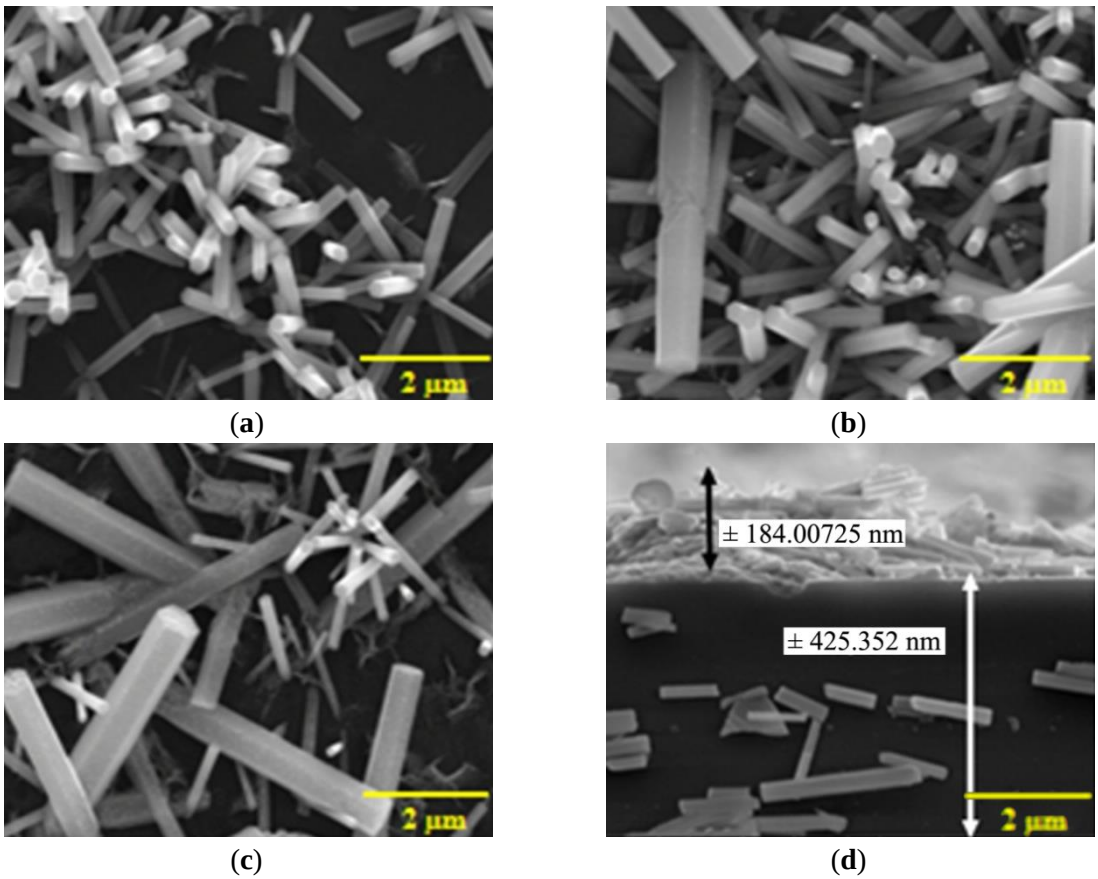

Figure 3. FESEM images of ZnO nanorods for (**a**) Z-3, (**b**) Z-6, (**c**) Z-9, and (**d**) Cross-section of ZnO.

The morphology of the Z-0 sample was not analyzed because it was only a ZnO seed. The distribution of the nanorods of the Z-3 sample (Figure 3, a) is quite uniform and shows the most homogeneous structure compared to other samples. Moreover, the nanorod is oriented in the vertical direction. Sample Z-6 (Figure 3, b) has a less homogeneous nanorod structure and a less uniform vertical orientation on the substrate. Sample Z-9 (Figure 3, c) reveals an inhomogeneous structure and diameter distribution of the ZnO nanorod, even though the orientation of the particles was found to be close to horizontal. The duration of ZnO growth demonstrates a decrease in the orientation of the nanorod in the vertical direction.

The histogram bar of ZnO nanorod size can be seen in Figure 4. The size distribution of nanorods is known from each sample's average diameter and standard deviation, which can be seen in Table 1. The longer the growth time, the larger the size of the ZnO nanorod. These results are in line with research reported by Mufti *et al.* (2022), who found that growth time increases particle size [40].

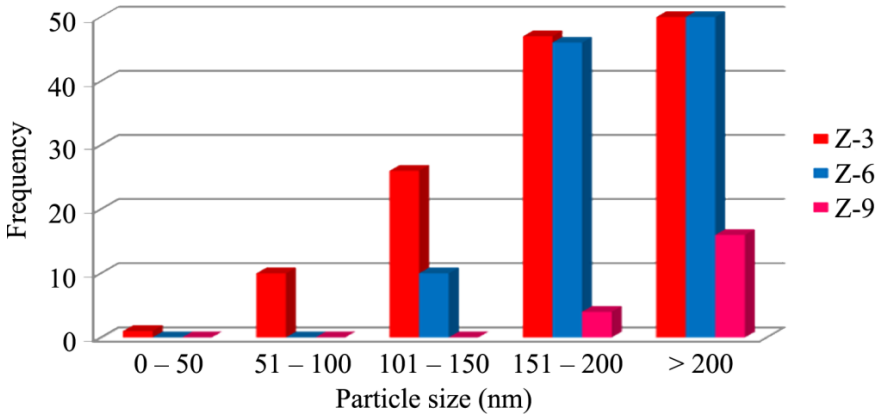

Figure 4. Histogram of ZnO nanorods sizes at different growth times.

Table 1. The size of ZnO nanorods.

Sample	Diameter (nm)
Z-3	142.68 ± 45.4
Z-6	169.57 ± 25.8
Z-9	203.92 ± 83.4

The cross-section side view (Figure 3, d) exhibits the dominantly oriented nanorod in the horizontal direction. The FESEM image shows a ZnO nanorod dominated by a hexagonal structure with a layer thickness of ± 184 nm and a substrate thickness of ± 425 nm. The decrease in the arrangement of ZnO nanorods in the vertical to horizontal direction was due to the increasing amount of reacting agents produced during the growth process, which resulted in the nanorod growing in the vertical and horizontal directions [41].

3.3. Crystal structure.

The X-ray diffraction pattern of the ZnO sample can be seen in Figure 5. The ZnO sample consists of diffraction peaks 2θ at 32.06º, 34.76º, 36.54º, 47.84º, 56.90º, 63.14º, 66.56º, and 68.16º correspond to the crystal planes (100), (002), (101), (102), (110), (103), and (210) respectively. Based on comparison with JCPDS data no. 36-1451, this pattern indicates the crystal structure of ZnO is hexagonal wurtzite [42].

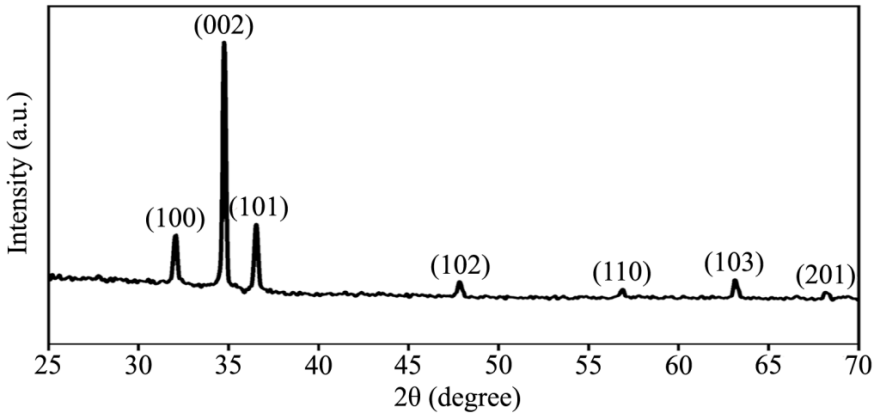

Figure 5. XRD pattern of sample ZnO.

Overall, the diffraction characteristics of the resulting ZnO phase have a relatively high peak intensity, and no other elemental phases were found in the XRD spectrum. The obtained ZnO crystal phase has lattice parameters a = b = 3.228 Å and c = 5.158 Å. It is consistent with the bulk ZnO lattice parameters, indicating that the growth orientation of the ZnO nanorods is in the direction of the c-axis on the (002) plane perpendicular to the surface of the glass substrate [43]. ZnO crystal size with the Scheerer formula was obtained at 39.98 nm with an FWHM of 0.217º. This value is in accordance with the previously reported by Abdulrahman *et al.* (2021) using the CBD method [33].

3.4. Self-cleaning test.

The self-cleaning ability of the ZnO sample can be seen from the contact angle of the water attached to the sample surface with wetting times of 0, 10, 20, and 30 minutes (Figure 6). The value of the water contact angle on the sample surface is shown in Table 2. Samples Z-0 and Z-3 have less hydrophobic properties because the contact angle is less than 90°. After wetting for up to 30 minutes, the water contact angle decreased from 63° to 43.3° and from 65.5° to 46.8° for each sample. So, the water spreads more over the surface and has hydrophilic

properties. Sample Z-6 exhibits hydrophobic properties with a water contact angle of 95.7°. After wetting for 10 and 20 minutes, the water contact angle was still hydrophobic (exceeding 90°). The hydrophobic surface is formed due to the high polarity of the surface so that water fills the grooves very easily through capillary action [44]. Sample Z-9 exhibits properties that are also hydrophobic with a water contact angle of 82.3º. However, after 30 minutes of wetting, the water contact angle decreased to 69.6º. These results are similar to a previously conducted by Shaban *et al*. (2017), where at 2 h of growth time, it has a contact angle of 35º, 4 h of growth time with a 40º, and 6 hours of growth time with an 85º contact angle. So, adding growth time increases the water contact angle with the sample surface [36].

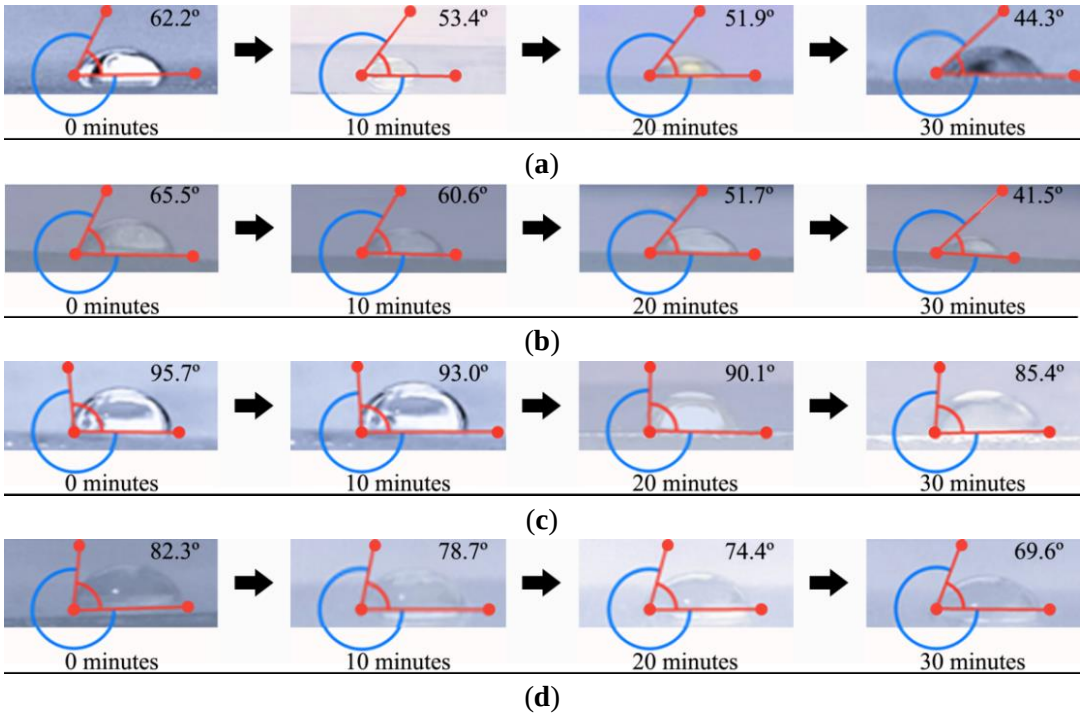

Figure 6. Self-cleaning test of sample for (**a**) Z-0, (**b**) Z-3, (**c**) Z-6, and (**d**) Z-9.

Table 2. Contact angle of ZnO sample.

Time (minute)	Contact Angle (degree)			
	Z-0	**Z-3**	**Z-6**	**Z-9**
0	62.2	65.5	95.7	82.3
10	53.4	60.6	93.0	78.7
20	51.9	51.7	90.1	74.4
30	44.3	41.5	85.4	69.6

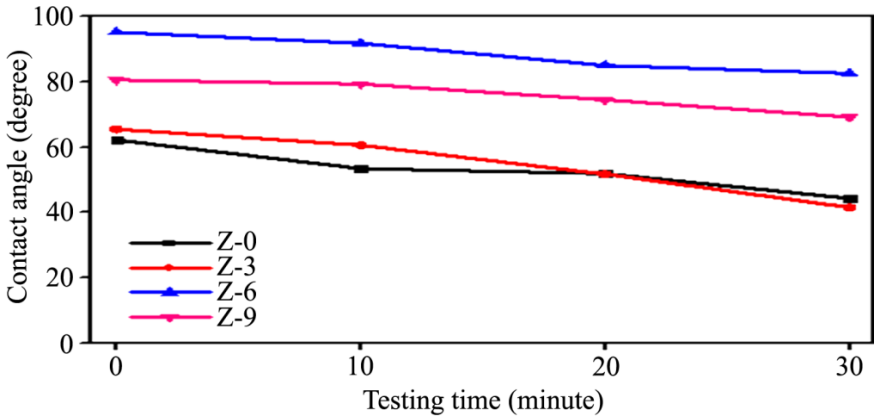

Figure 7. Contact angle curve of self-cleaning test.

The water contact angle curve against wettability time is shown in Figure 7. The largest water contact angle is found in sample Z-6. This is because the wettability of the sample surface involves surface roughness and surface energy that separates the water from the sample. The Z-6 sample has a homogeneous ZnO nanorod structure, such that the film growing on the substrate has the optimum roughness. The combination of increasing the roughness of the ZnO film structure and decreasing the surface energy during growth can increase the hydrophobicity ability [45].

The water contact angle that exceeds 90° makes ZnO samples potential for self-cleaning applications. Based on research reported by Valenzuela, for the application of self-cleaning glass, the surface of the material must be hydrophobic [46]. The hydrophobic makes water roll down with dirt so it doesn't stick to the glass, and the glass stays clean when exposed to water. The higher the water contact angle, the better the resulting hydrophobic properties, even reaching super hydrophobicity at a contact angle exceeding 150° [36].

4. Conclusions

ZnO nanorods prepared using the SILAR-CBD method by different growth times have been successfully synthesized. ZnO samples show maximum absorption in the ultraviolet region with high transmittance. ZnO nanorod has a diameter of ~169 nm with a hexagonal cross-section. The orientation of ZnO crystals with a wurtzite structure is obtained in the plane direction (002). The self-cleaning ability of the sample, with the best hydrophobic properties, was produced by Z-6 with a water contact angle of 95.7°. Growth time has affected the physical properties and self-cleaning ability of ZnO.

Funding

This work is funded by the Ministry of Education, Culture, Research, and Technology of the Republic of Indonesia (DRTPM) year 2023 research grant..

Acknowledgments

We thank the Riau University Research and Community Service Institute for supporting this research.

Conflicts of Interest

The authors declare no conflict of interest.

References

1. Banerjee, S.; Dionysiou, D.D.; Pillai, S.C. Self-cleaning applications of TiO_2 by photo-induced hydrophilicity and photocatalysis. *Appl Catal B Environ* **2015**, *176-177*, 396–428, https://doi.org/10.1016/j.apcatb.2015.03.058.
2. Rabajczyk, A.; Zielecka, M.; Klapsa, W.; Dziechciarz, A. Self-cleaning coatings and surfaces of modern building materials for the removal of some air pollutants. *Materials* **2021**, *14*, 2161, https://doi.org/10.3390/ma14092161.
3. Gao, Y.N.; Wang, Y.; Yue, T.N.; Weng, Y.X.; Wang, M. Multifunctional cotton non-woven fabrics coated with silver nanoparticles and polymers for antibacterial, superhydrophobic and high performance microwave shielding. *J of Colloid and Interface Sci* **2021**, *582*, 112–123, https://doi.org/10.1016/j.jcis.2020.08.037.
4. Wang, G.; Zhou, W.; Zhou, J.; Wang, M.; Zhang, Y.; Qiang, H. Superhydrophobic silicone rubber surface prepared by direct replication. *Surf Eng* **2021**, *37*, 278–287, https://doi.org/10.1080/02670844.2020.1776669.

5. Quan, Y.Y.; Chen, Z.; Lai, Y.; Huang, Z.S.; Li, H. Recent advances in fabricating durable superhydrophobic surfaces: a review in the aspects of structures and materials. *Mater Chemi Front* **2021**, *5*, 1655–1682, https://doi.org/10.1039/D0QM00485E.
6. Thi, T.U.D.; Nguyen, T.T.; Thi, Y.D.; Thi,K.H.T; Phan B.T.; Pham K.N. Green synthesis of ZnO nanoparticles using orange fruit peel extract for antibacterial activities. *RSC Adv* **2020**, *10*, 23899–23907, https://doi.org/10.1039/D0RA04926C.
7. Visali, C.; Priya, A.K.; Dharmaraj, R. Utilization of ecofriendly self-cleaning concrete using zinc oxide and polypropylene fibre. *Mater Today Proc* **2020**, *37*, 1083-1086, https://doi.org/10.1016/j.matpr.2020.06.309.
8. Zailan, S.N.; Mahmed, N.; Abdullah, M.M.A.B.; Rahim, S.Z.A.; Halin, D.S.C.; Sandu, A.V.; Vizureanu, P.; Yahya, Z. Potential applications of geopolymer cement-based composite as self-cleaning coating: A review. *Coatings* **2022**, *12*, 133, https://doi.org/10.3390/coatings12020133.
9. Wang, X.; Ding, H.; Wang, C.; Zhou, R.; Li, Y.; Li, W.; Ao, W. Self-healing superhydrophobic A-SiO_2/N-TiO_2@ HDTMS coating with self-cleaning property. *Appl Surf Sci* **2021**, *567*, 150808, https://doi.org/10.1016/j.apsusc.2021.150808.
10. Kang, E.S.; Kim, Y.W.; Nam, W.H. Multiple thermal resistance induced extremely low thermal conductivity in porous SiC-SiO_2 ceramics with hierarchical porosity. *J Eur Ceram Soc* **2021**, *41*, 1171-1180, https://doi.org/10.1016/j.jeurceramsoc.2020.10.004.
11. Xu, C.L.; Song, F.; Wang, X.L.; Wang. Y.Z. Surface modification with hierarchical CuO arrays toward a flexible , durable superhydrophobic and self-cleaning material. *Chem Eng J* **2017**, *313*, 1328–1334, https://doi.org/10.1016/j.cej.2016.11.024.
12. Mansor, M.L.H.A. ; Yunos, M.Z.; Harun, Z.; Hatta, M.N.M.; Hussin, R.; Ahmad, A.; Zulkefli A.S. Rheological and Thermodynamic Behaviour of PSf/ZnO: Effect of Zinc Oxide. *Int J Integr Eng* **2019**, *11*, 119–125, https://doi.org/10.30880/ijie.2019.11.05.016.
13. Wang, Y.; Baheti, V.; Khan, M.Z.; Viková, M.; Yang, K.; Yang, T.; Militký, J. A facile approach to develop multifunctional cotton fabrics with hydrophobic, self-cleaning and UV protection properties using ZnO particles and fluorocarbon. *J Text Inst* **2022**, *113*, 2238–2248, https://doi.org/10.1080/00405000.2021.1975905.
14. Wang, T.; Lu, Z.; Wang, X.; Zhang, Z.; Zhang, Q.; Yan, B.; Wang, Y. A compound of ZnO/PDMS with photocatalytic, self-cleaning and antibacterial properties prepared via two-step method. *Appl Surf Sci* **2021**, *550*, 149286, https://doi.org/10.1016/j.apsusc.2021.149286.
15. Kang, Z.; Ke, K.; Lin, E.; Qin, N.; Wu, J.; Huang, R.; Bao, D. Piezoelectric polarization modulated novel Bi_2WO_6/g-C_3N_4/ZnO Z-scheme heterojunctions with g-C_3N_4 intermediate layer for efficient piezo-photocatalytic decomposition of harmful organic pollutants. *J Colloid Interface Sci* **2022**, *607*, 1589–1602, https://doi.org/10.1016/j.jcis.2021.09.007.
16. Santhamoorthy, A.; Srinivasan, P.; Krishnakumar, A.; Rayappan, J.B.B.; Babu, K.Y. SILAR-deposited nanostructured ZnO thin films: effect of deposition cycles on surface properties. *Bull Mater Sci* **2021**, *44*, 188, https://doi.org/10.1007/s12034-021-02465-8.
17. Rashid, T.M.; Nayef, U.M.; Jabir, M.S.; Mutlak, F.A-H. Study of optical and morphological properties for Au-ZnO nanocomposite prepared by Laser ablation in liquid. *J Phys: Conf Ser* **2021** , *1795*, 012041, https://doi.org/10.1088/1742-6596/1795/1/012041.
18. Hasanpoor, M.; Aliofkhazraei, M.; Delavari, H. Microwave-assisted Synthesis of Zinc Oxide Nanoparticles. *Procedia Mater Sci* **2015**, *11*, 320–325, https://doi.org/10.1016/j.mspro.2015.11.101.
19. Rini, A.S.; Rati, Y.; Fadillah, R.; Farma, R.; Umar, L.; Soerbakti, Y. Improved Photocatalytic Activity of ZnO Film Prepared via Green Synthesis Method Using Red Watermelon Rind Extract. *Evergreen* **2022**, **9**, 1046–1055, https://doi.org/10.5109/6625718.
20. Ouslimane, T.; Et-Taya, L.; Elmaimouni, L.; Benami, A. Impact of absorber layer thickness, defect density, and operating temperature on the performance of $MAPbI_3$ solar cells based on ZnO electron transporting material. *Heliyon* **2021**, *7*, e06379, https://doi.org/10.1016/j.heliyon.2021.e06379.
21. Nurhasanah, I.; Efendi, A.F.; Sutanto, H.; Priyono. Growth and UV Absorption of 5 mol % Zn-doped CeO_2 Nanoparticle Synthesized with a Simple Precipitation Process. *Mater Sci Forum* **2015**, *827*, 62–66, https://doi.org/10.4028/www.scientific.net/MSF.827.62.
22. Pon, V.D.; Wilson, K.S.J.; Hariprasad, K.; Ganesh, V.; Ali, H.E.; Algarni, H.; Yahia, I.S. Enhancement of optoelectronic properties of ZnO thin films by Al doping for photodetector applications. *Superlattices Microstruct* **2021**, *151*, 106790, https://doi.org/10.1016/j.spmi.2020.106790.

23. Ramya, M.; Nideep, T.K.; Nampoori, V.P.N.; Kailasnath, M. Solvent assisted evolution and growth mechanism of zero to three dimensional ZnO nanostructures for dye sensitized solar cell applications. *Sci Rep* **2021**, *11*, 6159, https://doi.org/10.1038/s41598-021-85701-9.
24. Weldegrum, G.S.; Singh, P.; Huang, B.R.; Chiang, T.Y.; Tseng, K.W.; Yu, C.J.; Ji, C.; Chu, J.P. ZnO-NWs/metallic glass nanotube hybrid arrays: Fabrication and material characterization. *Surf Coat Technol* **2021**, *408*, 126785, https://doi.org/10.1016/j.surfcoat.2020.126785.
25. Hezam, M.; Alsubaie, M.Q.; Algarni, A.; Ghaithan, H.; Labis, J.; Alduraibi, M. ZnO Nanosheet-Nanowire morphology tuning for Dye-sensitized solar cell applications. *Chem Phys Lett* **2021**, *780*, 138953, https://doi.org/10.1016/j.cplett.2021.138953.
26. Liu, Y.; Li, Y.; Zeng, H. ZnO-Based Transparent Conductive Thin Films: Doping, Performance, and Processing. *J Nanomater* **2013**, *2013*, 196521, https://doi.org/10.1155/2013/196521.
27. Mazur, M.; Obstarczyk, A.; Posadowski, W.; Domaradzki, J.; Kiełczawa, S.; Wiatrowski, A.; Wojcieszak, D.; Kalisz, M.; Grobelny, M.; Szmidt, J. Investigation of the Microstructure, Optical, Electrical and Nanomechanical Properties of ZnOx Thin Films Deposited by Magnetron Sputtering. *Materials* **2022**, *15*, 6551, https://doi.org/10.3390/ma15196551.
28. Omerzu, A.; Peter, R.; Jardas, D.; Turel, I.; Salamon, K.; Podlogar, M.; Vengust, D.; Badovinac, I.J.; Piltaver, I.K.; Petravic, M. Large enhancement of photocatalytic activity in ZnO thin films grown by plasma-enhanced atomic layer deposition. *Surf Interfaces* **2021**, *23*, 100984, https://doi.org/10.1016/j.surfin.2021.100984.
29. Sánchez-Martín, S.; Olaizola, S.M.; Castaño, E.; Urionabarrenetxea, E.; Mandayo, G.G.; Ayerdi, I. Study of deposition parameters and growth kinetics of ZnO deposited by aerosol assisted chemical vapor deposition. *RSC Adv* **2021**, *11*, 18493–18499, https://doi.org/10.1039/D1RA03251H.
30. Nwanna, E.C.; Bitire, S.; Imoisili, P.E.; Jen, T.C. An overview of the application of atomic layer deposition process for lithium-ion based batteries. *Int J Energy Res* **2022**, *46*, 10499–10521, https://doi.org/10.1002/er.7941.
31. Moumen, A.; Kumarage, G.C. W.; Comini, E. P-type Metal Oxide Semiconductor Thin Films: Synthesis and Chemical Sensor Applications. *Sensors* **2022**, *22*, 1359, https://doi.org/10.3390/s22041359.
32. Macías-Cabrera, C.A.; Campos-Álvarez, J.; Gamboa, S.A.; Aguilar-Martínez, J.A.; Peña-Méndez, Y. Synthesis of CZTS thin films from binary precursors stacking by chemical bath deposition for solar cell applications. *Mater Today: Proc* **2021,** *46*, 3109–3113, https://doi.org/10.1016/j.matpr.2021.02.624.
33. Abdulrahman, A.F.; Ahmed, S.M.; Barzinjy, A.A.; Hamad, S.M.; Ahmed, N.M.; Almessiere, M.A. Fabrication and Characterization of High-Quality UV Photodetectors Based ZnO Nanorods Using Traditional and Modified Chemical Bath Deposition Methods. *Nanomaterials* **2021**, *11*, 677, https://doi.org/10.3390/nano11030677.
34. Dhaygude, H.D.; Shinde, S.K.; Velhal, N.B.; Lohar, G.M.; Fulari, V.J. Synthesis and characterization of ZnO thin film by low cost modified SILAR technique. *AIMS Mater Sci* **2016**, *3*, 349–356, https://doi.org/10.3934/matersci.2016.2.349.
35. Krishnan, D.; Sreedev, P.; Rakhesh, V.; Roshima, N.S.; Shankar, B.; Sunil M. Comparative optical study of ZnO thin films prepared by SILAR method. *AIP Conf Proc* **2019**, *2162*, 020132, https://doi.org/10.1063/1.5130342.
36. Shaban, M.; Zayed, M.; Hamdy, H. Nanostructured ZnO thin films for self-cleaning applications. *RSC Adv* **2017**, *7*, 617–631, https://doi.org/10.1039/C6RA24788A.
37. Humayun, Q.; Kashif, M.; Hashim, U.; Qurashi, A. Selective growth of ZnO nanorods on microgap electrodes and their applications in UV sensors. *Nanoscale Res Lett* **2014**, *9*, 29, https://doi.org/10.1186/1556-276X-9-29.
38. Chen, C.; Zheng, S.; Song, H. Photon management to reduce energy loss in perovskite solar cells. *Chem Soc Rev* **2021**, *50*, 7250–7329, https://doi.org/10.1039/D0CS01488E.
39. Quintanilla, M.; Hemmer, E.; Marques-Hueso, J.; Rohani, S.; Lucchini, G.; Wang, M.; Zamani, R.R.; Roddatis, V.; Speghini, A.; Richards, B.S.; Vetrone, F. Cubic versus hexagonal–phase, size and morphology effects on the photoluminescence quantum yield of $NaGdF_4$: Er^{3+}/Yb^{3+} upconverting nanoparticles. *Nanoscale* **2022**, *14*, 1492–1504, https://doi.org/10.1039/D1NR06319G.
40. Mufti, N.; Sari, E.T.; Abadi, M.T.H.; Dewi, A.S.P.; Diantoro, M.; Aziz, M.S.; Zulhadjri; Setiyanto, H.; Sunaryono; Puspitasari, P. Effect of activation temperature of Yttria Stabilized Zirconia (YSZ)/ZnO nanorods thin film on photoelectrochemical cell performance. *J Mater Res Technol* **2022**, *20*, 2348–2357, https://doi.org/10.1016/j.jmrt.2022.07.173.

41. Yuwono, A.H.; Suhaimi, L.; Sofyan, N.; Dhaneswara,D. ; Ramahdita,G.;Sholehah, A.; Hudaya, C. Nanostructural Growth Investigation of Zno Nanorods Derived from Chemical Bath Deposition for Transparent Heater Application. *Int J Technol* **2018**, *9*, 1216–1224, https://doi.org/10.14716/ijtech.v9i6.2452.
42. Ruhaizat, N.E.; Ainuddin, A.R.; Kamdi, Z. Experimental the Influence of Growth Solution on Zinc Oxide Crystal Structures via Hydrothermal Method. *Int J Integr Eng* **2021**, *13*, 222–228.
43. Terasako, T.; Hamamoto, K.; Yagi, M.; Furubayashi, Y.; Yamamoto, T. Structural and photoluminescence properties of zinc oxide nanorods grown on various transparent conducting oxide seed layers by chemical bath deposition. *Thin Solid Films* **2021**, *732*, 138803, https://doi.org/10.1016/j.tsf.2021.138803.
44. Wang, Y.; Li, B.; Liu, T.; Xu, C.; Ge, Z. Controllable fabrication of superhydrophobic TiO_2 coating with improved transparency and thermostability. *Colloids Surf A Physicochem Eng Asp* **2014**, *441*, 298–305, https://doi.org/10.1016/j.colsurfa.2013.09.023.
45. Milionis, A.; Tripathy,A.; Donati,M.; Sharma,C.S.; Pan,F.; Maniura-Weber,K.; Ren,Q.; Poulikakos,D. Water-Based Scalable Methods for Self-Cleaning Antibacterial ZnO-Nanostructured Surfaces. *Ind Eng Chem Res* **2020**, *59*, 14323–14333, https://doi.org/10.1021/acs.iecr.0c01998.
46. Valenzuela, L.; Iglesias, A.; Faraldos, M.; Bahamonde, A.; Rosal, R. Antimicrobial surfaces with self-cleaning properties functionalized by photocatalytic ZnO electrosprayed coatings. *J Hazard Mater* **2019**, *369*, 665–673, https://doi.org/10.1016/j.jhazmat.2019.02.073.